Biomaterials Science

ROYAL SOCIETY OF CHEMISTRY

PAPER

View Article Online
View Journal | View Issue



Cite this: *Biomater. Sci.*, 2024, **12**, 4386

# Halogen atom regulation of acceptor–donor–acceptor type conjugated molecules for photothermal antibacterial and antibiofilm therapy†

Yue Zhao,[a] Yuanyuan Cui,[a] Shijie Xie,[b] Ruilian Qi,[a] Li Xu *[b] and Huanxiang Yuan *[a]

Drug-resistant bacteria and biofilm have caused serious public health problems. It is necessary to develop a treatment that is highly effective against drug-resistant bacteria without inducing drug resistance. Herein, we prepare a series of nanoparticles based on three conjugated molecules (BTP-BrCl, BTP-ClBr, and BTP-ClmBr) with acceptor–donor–acceptor (A–D–A) structure. By adjusting the position of the halogen atoms, the photothermal properties can be effectively regulated. In particular, these three nanoparticles (BTP-BrCl, BTP-ClBr, and BTP-ClmBr NPs) exhibited photothermal conversion efficiencies (PCE) up to 57.4%, 60.3%, and 75.9%, respectively. Among these nanoparticles, BTP-ClmBr NPs with the chlorine atom close to the carbonyl and the bromine atom away from the carbonyl in the acceptor have the highest PCE. Due to their excellent photothermal properties, all the NPs achieved more than 99.9% antibacterial activity against Amp$^r$ *E. coli*, *S. aureus* and MRSA. When *S. aureus* was treated with these three nanoparticles under light irradiation, little biofilm formation was observed. Moreover, they could kill more than 99.9% of the bacteria in the biofilm. In summary, this study provides a strategy for the preparation of high-performance nano-photothermal agents and their application in the field of anti-drug resistant bacteria and biofilm prevention and cure.

Received 30th April 2024,
Accepted 12th July 2024

DOI: 10.1039/d4bm00605d

rsc.li/biomaterials-science



## Introduction

The abuse of antibiotics has led to the emergence of a large number of drug-resistant bacteria, making the related infectious diseases difficult to cure. In 2019, resistance genes were discovered in the Arctic, suggesting that resistant bacteria have spread to remote parts of the planet.[1] According to a report in The Lancet, it was estimated that about 1.27 million people will die due to drug-resistant bacteria in 2019.[2] If the resistance situation cannot be controlled, the number of deaths is predicted to exceed 10 million by 2050.[3] Bacteria tend to aggregate and form more intractable biofilms of microbial communities. Polymers secreted by bacteria, such as proteins and polysaccharides, can form extracellular polymers (EPS), which are more resistant to most conventional treatments.[4] Therefore, it is extremely necessary to develop a treatment that is highly effective against bacteria and destroys biofilms without causing resistance.

At present, the common treatment methods include phototherapy, sonodynamic therapy and chemodynamic therapy.[5–9] Among them, phototherapy encompasses photodynamic therapy and photothermal therapy (PTT). PTT refers to the denaturation of macromolecules such as proteins and DNA by heating under the excitation of a light source to kill bacteria.[10,11] The excitation source usually used is near-infrared light with a penetration depth of 1–2 cm.[12] Since this therapy achieves its antibacterial purpose by directly destroying the bacterial structure, it will not be affected by drug resistance, nor will it induce the generation of drug-resistant bacteria. In addition, due to the advantages of non-invasive, high biological safety and low invasiveness, photothermal therapy has been widely used in the treatment of drug-resistant bacterial infections.[13]

In PTT, the choice of photothermal agent is important. In practical application, photothermal agents should meet the following requirements:[14,15] (1) excellent photothermal pro-

[a]*Department of Chemistry, College of Chemistry and Materials Engineering, Beijing Technology and Business University, Beijing 100048, China. E-mail: yhx@iccas.ac.cn*
[b]*Department of Pharmacy, Hubei University of Chinese Medicine, Wuhan 430065, China*

†Electronic supplementary information (ESI) available. See DOI: https://doi.org/10.1039/d4bm00605d

perties, including photothermal conversion ability, photothermal stability and temperature tunability; (2) good biosafety and *in vivo* degradability; (3) easy preparation and synthesis. At present, there are a variety of materials with photothermal conversion ability have been found, including inorganic materials, organic materials and organic–inorganic composite materials. Inorganic materials include carbon-based materials (graphene), metallic materials (silver and gold), and metallic sulfides.[16–18] Although inorganic materials have excellent photothermal conversion ability, they are limited by degradation performance and low biological safety, which hinders them widely used in clinical applications.[19] Organic materials, especially organic molecules, are relatively safe and easy to be degraded, but poor photothermal stability and difficulty in synthesis are still difficulties.

Structurally determined organic conjugated molecules exhibit better light capture.[20] According to the energy gap law, the introduction of A–D–A structure is beneficial to enhance intramolecular charge transfer and reduce the band gap of conjugated molecules, effectively inhibit fluorescence, and enhance the non-radiative decay of molecules. In addition, A–D–A structure usually also exhibits extensive absorption extending into the NIR region.[21] Photothermal agents with excellent performance are usually obtained by regulating the electron withdrawing ability of the acceptor or the electron donating ability of the donor. Organic conjugated molecules can also be prepared into nanoparticles, which can improve biocompatibility while maintaining their good photothermal conversion capacity. Therefore, it is an efficient solution to design organic conjugated nanoparticles with A–D–A structure for the treatment of diseases caused by drug-resistant bacterial infections.

Herein, we prepared a series of nanoparticles based on three conjugated molecules with A–D–A structures, where the position of halogen atoms on the acceptor moieties varied. All three organic conjugated molecules use benzothiadiazole as the electron donor. By regulating the position of the halogen atom on the acceptor group, the electron withdrawing ability can be changed, and then the photothermal conversion ability can be adjusted. According to the different positions of Br and Cl on the benzene ring, the three molecules were named BTP-BrCl, BTP-ClBr, and BTP-ClmBr. Based on this, we tested the photothermal properties of these three nanoparticles and explored their potential application in antibacterial and anti-biofilm applications.

## Results and discussion

### Synthesis and characterization

BTP-BrCl, BTP-ClBr, and BTP-ClmBr were synthesized according to the previous report.[22] Both BTP-BrCl and BTP-ClBr have the acceptor with chlorine and bromine atoms in the *ortho* relationship. The difference is that the bromine atom in BTP-BrCl is closer to the carbonyl group in the acceptor, while the chlorine atom in BTP-ClBr is closer to the carbonyl group. While the chlorine and bromine atoms in BTP-ClmBr are in *meta* relationship and the chlorine atom is closer to the carbonyl group. To improve the water dispersion and biomedical applications of BTP-BrCl, BTP-ClBr, and BTP-ClmBr, an amphiphilic molecule PEG-DSPE2000 with a long alkyl tail and a hydrophilic head group was used as the encapsulation matrix. The corresponding nanoparticles were prepared by nano-coprecipitation (Scheme 1b).[23] The UV absorption

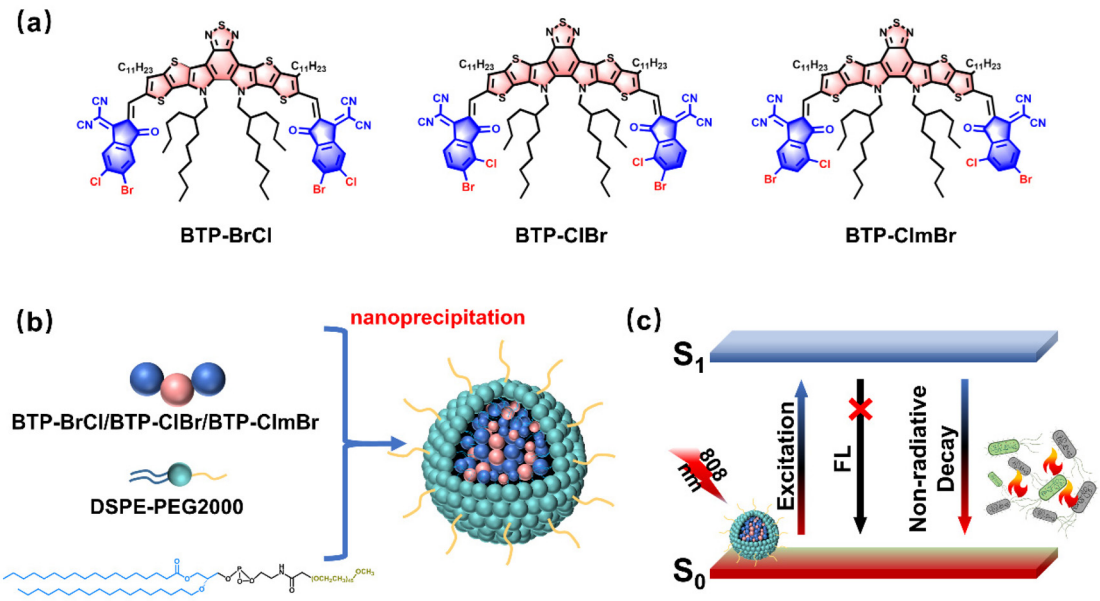


**Scheme 1** (a) Chemical structures of the conjugated molecule. (b) Preparation of nanoparticles. (c) Schematic diagram of nanoparticles photothermal antibacterial therapy.

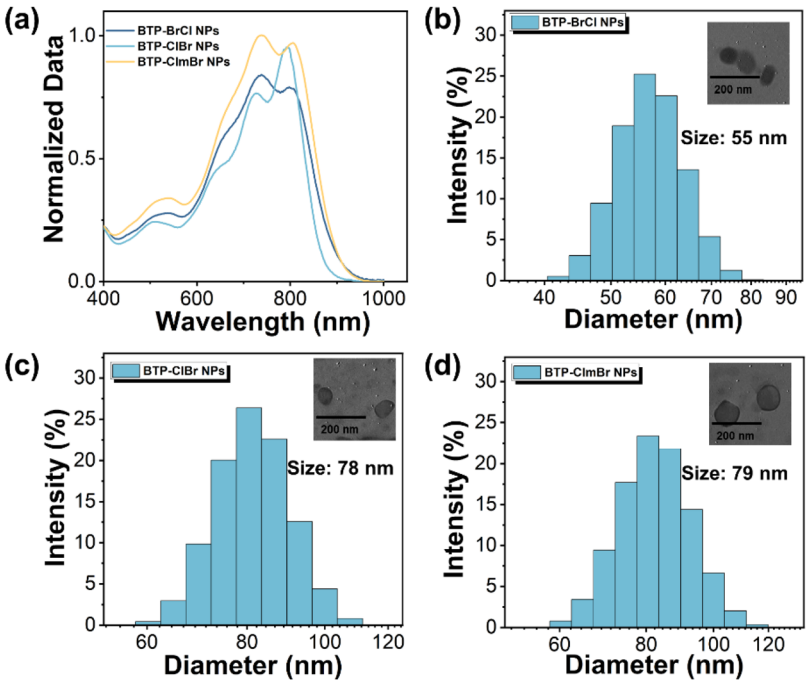


**Fig. 1** (a) Normalized absorption spectra of BTP-BrCl/BTP-ClBr/BTP-ClmBr NPs. Size distribution and corresponding TEM images (in the set) of (b) BTP-BrCl NPs, (c) BTP-ClBr NPs and (d) BTP-ClmBr NPs.

spectra in Fig. 1a shows that the BTP-BrCl/BTP-ClBr/BTP-ClmBr NPs have a wide UV absorption in the range of 600 to 900 nm. Specifically, the BTP-ClmBr NPs have a stronger absorption near 800 nm, which is due to the stronger electron withdrawing ability of its acceptor structure. According to the results of dynamic light scattering (DLS) measurement, the hydrodynamic diameters of BTP-BrCl/BTP-ClBr/BTP-ClmBr NPs were 55 nm, 78 nm and 79 nm, respectively (Fig. 1b–d). TEM images showed that these NPs were uniformly distributed spherical morphology.

### Characterization of photothermal properties

Subsequently, the photothermal conversion ability of BTP-BrCl/BTP-ClBr/BTP-ClmBr NPs was investigated. Under the 808 nm laser irradiation (800 mW $cm^{-2}$), the water dispersion of these three NPs (10 μg $mL^{-1}$) showed a rapid upward trend, and the temperature changed by 57.3 °C, 58.1 °C and 62.4 °C after 5 min of illumination, respectively (Fig. 2a). And the temperature of the blank group (ultrapure water) remained almost unchanged. The warming infrared thermogram is shown in Fig. 2g, Fig. S1f, and S2f.† It can be concluded that BTP-ClmBr NPs have stronger intramolecular charge transfer, enhanced non-radiative transition, and stronger photothermal conversion ability. It is shown that the position of halogen atom can affect the electron withdrawing ability of electron acceptor, and then can regulate the photothermal properties of A–D–A type molecule. To further demonstrate the potential of photothermal conversion, the temperature variation of NPs at different concentrations (12.5, 25, 50, 100 μg $mL^{-1}$) was measured under 808 nm laser irradiation (1 W $cm^{-2}$) for 5 min (Fig. 2b and Fig. S1a, and S2a†). It can be seen that the temperature of the aqueous solution of NPs elevated significantly with the concentration increasing. In addition, laser with different light intensities (0.5, 0.75, 1, 1.5 W $cm^{-2}$) was used to irradiate the 25 μg $mL^{-1}$ NPs aqueous solution. With the increase of light intensity, the photothermal conversion ability was also enhanced (Fig. 2c and Fig. S1b, S2b†). Therefore, the photothermal conversion of NPs can be regulated by adjusting the light intensity and concentration to effectively prevent thermal damage. As shown in Fig. 2d and Fig. S1c, S2c,† the NPs solution (10 μg $mL^{-1}$) was irradiated with 808 nm NIR light (800 mW $cm^{-2}$) for 5 min, and naturally cooled to room temperature for ON/OFF laser irradiation cycle. The photothermal conversion capacity remained well after five cycles, indicating that the BTP-BrCl/BTP-ClBr/BTP-ClmBr NPs have excellent photothermal stability and can be recycled. The temperature changes of the NPs in the irradiated (5 min) and laser off state (5 min) were recorded under the same laser conditions (Fig. 2e, f and Fig. S1d, S1e, S2d, S2e†), and the PCE of BTP-BrCl/BTP-ClBr/BTP-ClmBr NPs was determined to be 57.4%, 60.3%, and 75.9%.

### Antibacterial measurement

To evaluate the antimicrobial effects of the three NPs, $Amp^r$ *E. coli* was used as a representative of Gram-negative bacteria. $Amp^r$ *E. coli* was incubated with NPs of different concentration gradients (5, 7.5, 10 μg $mL^{-1}$) for 30 min in the dark (37 °C) and irradiated with an 808 nm laser at 550 mW $cm^{-2}$ for 5 min. As can be seen from the plate in Fig. 3e, the blank group under illumination without NPs did not show signifi-

 

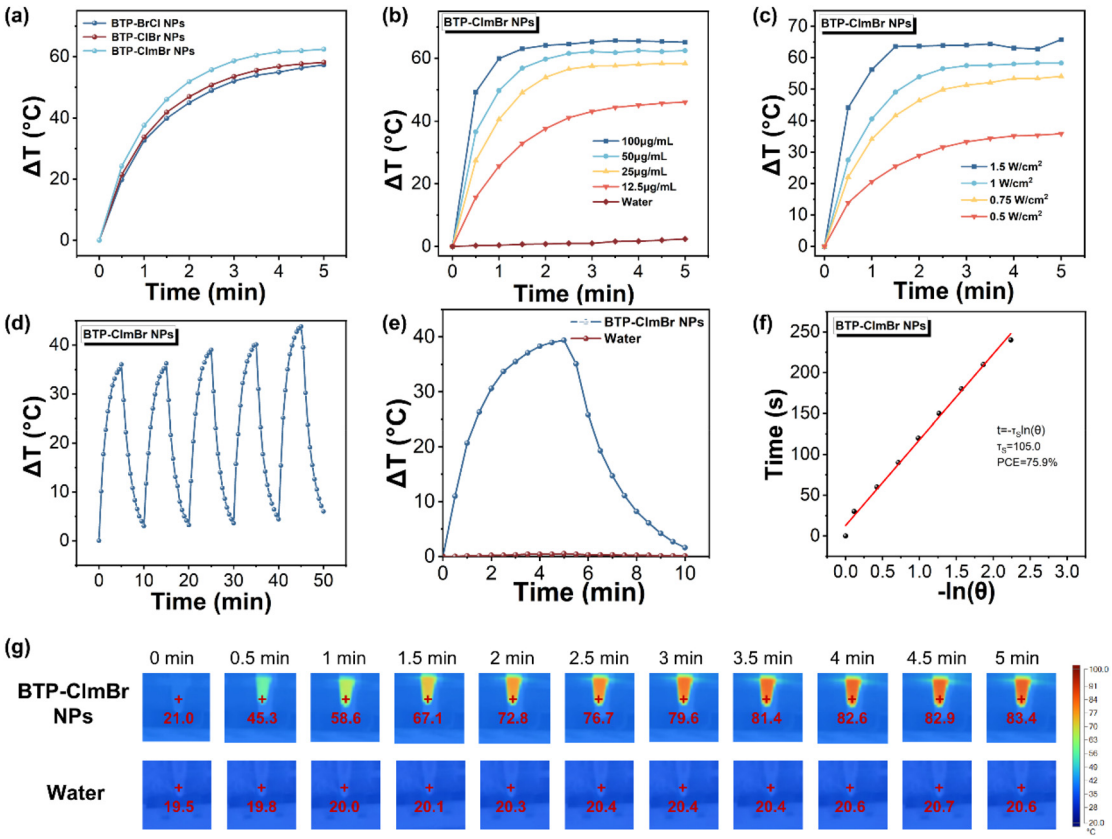


**Fig. 2** (a) Temperature increase of water and different nanoparticles (10 μg $mL^{-1}$) after 808 nm laser irradiation (800 mW $cm^{-2}$) for 5 min. (b) Heating curves of water dispersions of BTP-ClmBr NPs at different concentrations irradiated by 808 nm laser (1 W $cm^{-2}$). (c) Heating curves of water dispersions of BTP-ClmBr NPs (25 μg $mL^{-1}$) at different laser power densities. (d) Heating and cooling cycle curves of five ON/OFF cycles of BTP-ClmBr NPs dispersed (10 μg $mL^{-1}$) under 808 nm laser irradiation (800 mW $cm^{-2}$). (e and f) Photothermal properties of BTP-ClmBr NPs after cooling to room temperature. (g) Infrared thermogram of BTP-ClmBr NPs (10 μg $mL^{-1}$) increasing with irradiation time (808 nm, 800 mW $cm^{-2}$).

cant difference from the dark condition, indicating that the laser itself had no impact on bacteria. The three NPs showed almost no dark toxicity to bacteria under dark conditions, indicating their good biocompatibility. In addition, when the concentration of BTP-BrCl/BTP-ClBr/BTP-ClmBr was 10 μg $mL^{-1}$, the antibacterial rate could reach more than 99.9% after 5 minutes of laser irradiation (Fig. 3a and Fig. S3a, S4a†). Subsequently, the antibacterial effects of BTP-BrCl/BTP-ClBr/BTP-ClmBr NPs against Gram-positive bacteria (*S. aureus* and MRSA) were investigated under the same laser irradiation conditions. The results showed that when the concentration was 10 μg $mL^{-1}$, the inhibition rate of NPs toward these two bacteria could also reach more than 99.9% (Fig. 3b, c and Fig. S3b, S3c, S4b, S4c†), demonstrating the excellent antibacterial activity against resistant bacteria.

To further understand the antibacterial behavior of the NPs, the bacterial morphology after various treatments was characterized by scanning electron microscopy (SEM). As shown in Fig. 3f and Fig. S3f, S4f,† the bacteria in the blank control group had complete morphology and clear edges. Bacterial morphology remained unchanged after interaction with BTP-ClmBr NPs under dark conditions. After 5 min of laser irradiation, the bacteria gradually showed more collapses and holes as the concentration of NPs increased. The same experimental results were observed for BTP-BrCl/BTP-ClBr NPs against $Amp^r$ *E. coli*, *S. aureus* and MRSA. This phenomenon is consistent with the results of antibacterial experiments, which showed that NPs exhibited excellent killing effects against drug-resistant bacteria $Amp^r$ *E. coli* and MRSA. Therefore, BTP-BrCl/BTP-ClBr/BTP-ClmBr NPs are primiarily achieve antibacterial effects by generating high temperatures that disrupt bacterial structures.

### Effect of biofilm inhibition/destruction

To further explore the long-term inhibitory effect of BTP-BrCl/BTP-ClBr/BTP-ClmBr NPs on bacteria, a *S. aureus* biofilm model was constructed. The samples treated with NPs after irradiation were cultured to investigate whether a biofilm could form, which demonstrate the long-term antibacterial activity of these photothermal nanoparticles. 20 μL of *S. aureus* bacterial solution was mixed with 20 μg $mL^{-1}$ BTP-BrCl/BTP-ClBr/BTP-ClmBr NPs and incubated for 30 min in the dark. After laser irradiation at 808 nm, 550 mW $cm^{-2}$ for 5 min, the processed samples were supplemented with

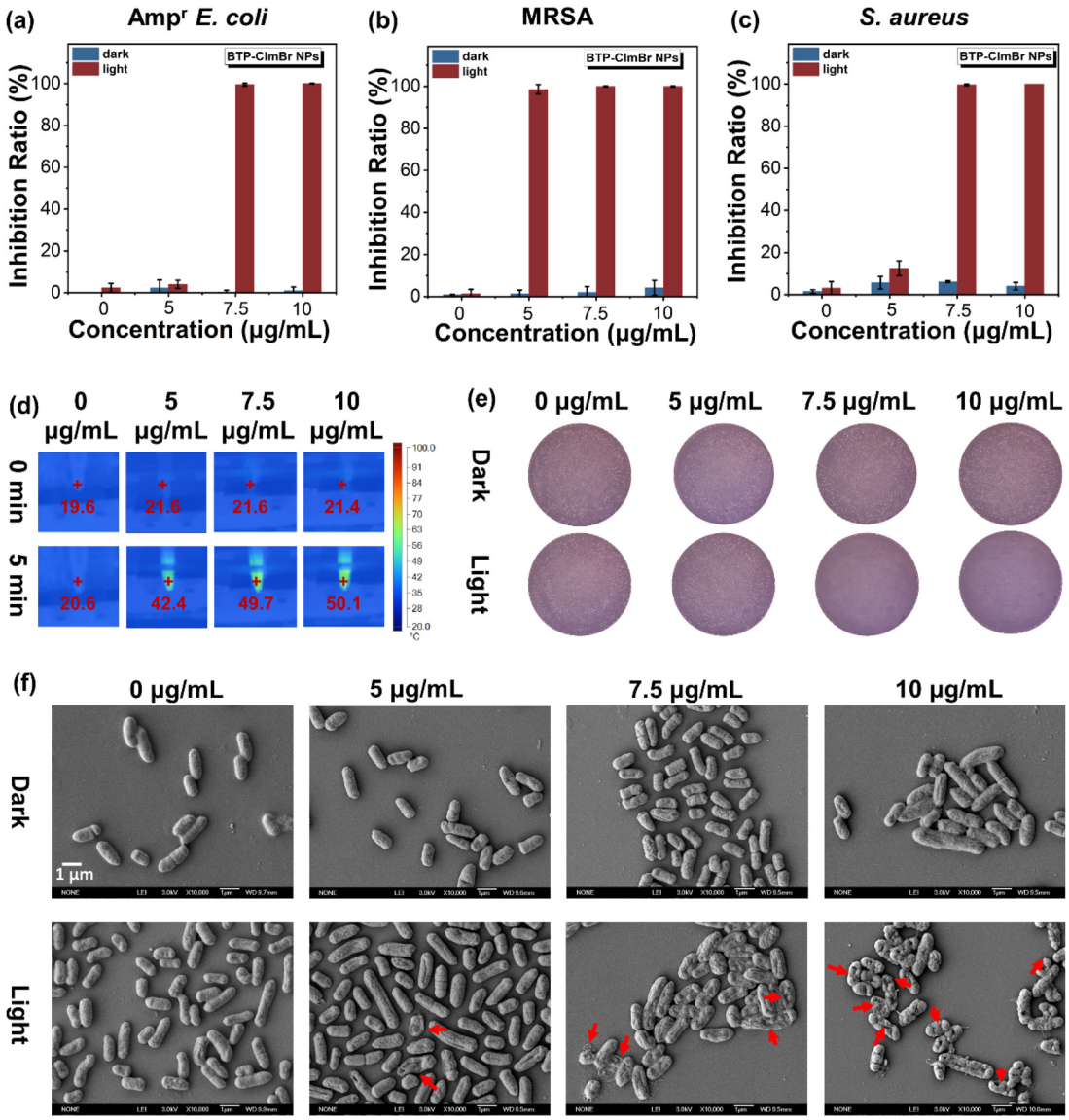


**Fig. 3** Antibacterial activity of BTP-ClmBr NPs against (a) Amp$^r$ *E. coli*, (b) *S. aureus*, and (c) MRSA in the dark or irradiated with 808 nm laser (550 mW cm$^{-2}$) for 5 min. (d) Corresponding infrared thermograms of Amp$^r$ *E. coli* treated with different concentrations of BTP-ClmBr NPs at 0 and 5 min of irradiation; (e) photographs of Amp$^r$ *E. coli* solid plates treated with different concentrations of BTP-ClmBr NPs. (f) SEM images of Amp$^r$ *E. coli* treated with different concentrations of BTP-ClmBr NPs. Scale bar: 1 μm.

medium and further cultured to observe the formation of biofilms. Crystal violet staining was used to analyze the growth of biofilm. Fig. 4a shows that biofilm growth after treatment with BTP-BrCl/BTP-ClBr/BTP-ClmBr NPs was less than 5% after 12 h and 18 h of culture. After 24 hours of culture, the inhibition rate of BTP-BrCl NPs with relatively poor antibacterial effect on biofilm was 36.01%. However, the inhibition of the biofilm by BTP-ClBr NPs and BTP-ClmBr NPs was still higher than 94%. This indicated that all three NPs were able to effectively kill bacteria to further inhibit biofilm formation.

The antimicrobial properties of BTP-BrCl/BTP-ClBr/BTP-ClmBr NPs against mature biofilms were further evaluated. *S. aureus* mature biofilm that had been cultured for 24 h were incubated with BTP-BrCl, BTP-ClBr and BTP-ClmBr NPs respectively at the concentration of 15 μg mL$^{-1}$ for 30 min. After exposure to 808 nm laser at 1 W cm$^{-2}$ for 10 min, the biofilms were stained and the remaining bacteria was characterized using the plate counting method. Although the biofilm was not completely destroyed (Fig. 4b and c), the bacterial mortality in it could reach more than 99.9% (Fig. 4d). As can be seen from Fig. 4e, there was no colony formation on the medium. In conclusion, BTP-BrCl/BTP-ClBr/BTP-ClmBr NPs could inhibit or destroy biofilm formation by heating up under NIR light irradiation. In addition, the hemolysis rates of BTP-BrCl/BTP-ClBr/BTP-ClmBr NPs for rabbit blood (obtained from Beijing Jinlisi Technology Co., Ltd) were all much lower than 5% (Fig. 5a–c), indicating that they have good blood compatibility and have the potential for clinical application.

 

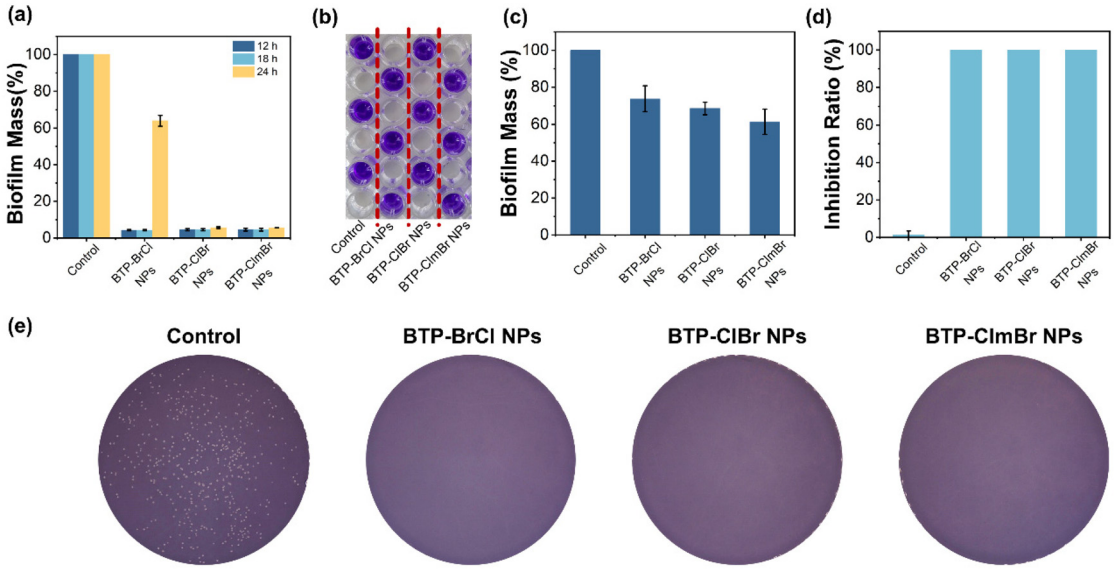


**Fig. 4** (a) The corresponding biofilm biomass (OD = 590 nm) was determined by crystal violet staining absorbance. *S. aureus* (808 nm, 550 mW $cm^{-2}$) was treated with BTP-BrCl/BTP-ClBr/BTP-ClmBr NPs (10 μg $mL^{-1}$) and cultured for 12, 18, and 24 h, respectively. (b) Crystal violet staining images of the corresponding biofilm. (c) Biofilm biomass (OD = 590 nm) after anti-biofilm treatment. *S. aureus* biofilms were treated with PBS and BTP-BrCl/BTP-ClBr/BTP-ClmBr NPs (15 μg $mL^{-1}$) for 10 min using 808 nm laser (1.0 W $cm^{-2}$). (d) The corresponding antimicrobial tests. (e) Pictures of *S. aureus* solid plates.

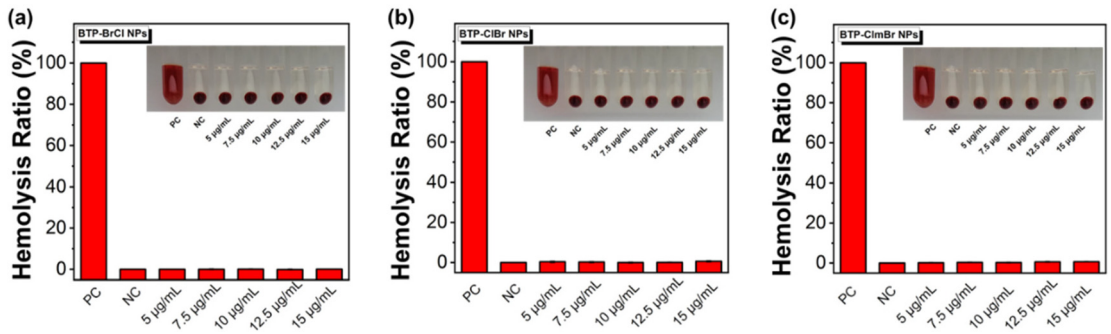


**Fig. 5** Hemolysis rates and corresponding images (in the set) of (a) BTP-BrCl NPs, (b) BTP-ClBr NPs, and (c) BTP-ClmBr NPs.

## Conclusion

In summary, we have proposed a strategy to modulate the electron withdrawing ability by changing the position of halogen atoms on the acceptor structure, and have successfully synthesized nanoparticles based on three organic conjugated molecules (BTP-BrCl, BTP-ClBr, and BTP-ClmBr) with A–D–A structure. These NPs can effectively convert near-infrared light to heat. Among them, the acceptor structure with chlorine and bromine atoms at *ortho*-position in BTP-ClmBr has the strongest electron absorbing ability, embowing BTP-ClmBr NPs the greatest near-infrared absorption and photothermal conversion ability. The antibacterial experiment showed that only 10 μg $mL^{-1}$ of BTP-BrCl/BTP-ClBr/BTP-ClmBr NPs could achieve 99.9% antibacterial effect ($Amp^r$ *E. coli*, *S. aureus*, and MRSA). After treatment with 20 μg $mL^{-1}$ of nanoparticles, the formation of biofilms can be greatly inhibited. At the same time, the mortality ratio of bacteria in the biofilm was more than 99.9% after treatment with 15 μg $mL^{-1}$ of BTP-BrCl/BTP-ClBr/BTP-ClmBr NPs. Therefore, these nanoparticles could both effectively kill bacteria and inhibit the formation of biofilms. In addition, these three NPs showed low dark toxicity and excellent blood compatibility, which suggested their potential for clinical application. In conclusion, the design strategy of improving the photothermal conversion ability of A–D–A skeleton organic conjugated molecules by adjusting the acceptor structure provides certain implications for the development of photothermal agents to combat clinical drug resistant bacterial infections.

## Author contributions

Yue Zhao: conceptualization, methodology, investigation, software, writing-original draft preparation. Yuanyuan Cui, Shijie

Xie: methodology. Ruilian Qi: visualization, investigation. Li Xu: methodology, supervision. Huanxiang Yuan: conceptualization, methodology, supervision, writing-reviewing and editing.

## Data availability

The data supporting this article have been included as part of the ESI.†

## Conflicts of interest

There are no conflicts to declare.

## Acknowledgements

The authors are gratefully acknowleged for the project of Cultivation for young top-notch talents of Beijing Municipal Institutions (BPHR202203045).



## References

1 M. Piksa, C. Lian, I. C. Samuel, K. J. Pawlik, I. D. W. Samuel and K. Matczyszyn, *Chem. Soc. Rev.*, 2023, **52**, 1697–1722.
2 M. Xie, M. Gao, Y. Yun, M. Malmsten, V. M. M. Rotello, R. Zboril, O. Akhavan, A. Kraskouski, J. Amalraj, X. Cai, J. Lu, H. Zheng and R. Li, *Angew. Chem., Int. Ed.*, 2023, **62**, e202217345.
3 T. Pulingam, T. Parumasivam, A. M. Gazzali, A. M. Sulaimana, J. Y. Chee, M. Lakshmanan, C. F. Chin and K. Sudesh, *Eur. J. Pharm. Sci.*, 2022, **170**, 106103.
4 J. Li, G. Pan, G. V. Zyryanov, Y. Peng, G. Zhang, L. Ma, S. Li, P. Chen and Z. Wang, *ACS Appl. Mater. Interfaces*, 2023, **15**, 40864–40876.
5 S. Singh, W. E. Meador, A. Pramanik, P. Ray, J. H. Delcamp and Y. Zhao, *J. Photochem. Photobiol., B*, 2023, **240**, 112652.
6 J. Jiang, X. Lv, H. Cheng, D. Yang, W. Xu, Y. Hu, Y. Song and G. Zeng, *Acta Biomater.*, 2024, **177**, 1–19.
7 W. Guo, Y. Wang, K. Zhang, X. Dai, Z. Qiao, Z. Liu, B. Yu, N. Zhao and F.-J. Xu, *Chem. Mater.*, 2023, **35**, 6853–6864.
8 M. Yang, M. Xie, J. Guo, Y. Zhang, Y. Qiu, Z. Wang and Y. Du, *Int. J. Nanomed.*, 2023, **18**, 7941–7963.
9 Q. Chen, M. Qi, F. Shi, C. Liu, Y. Shi, Y. Sun, X. Bai, L. Wang, X. Sun, B. Dong and C. Li, *Adv. Healthcare Mater.*, 2023, **12**, 2300313.
10 W. He, Z. Wang, H. Bai, Z. Zhao, R. T. K. Kwok, J. W. Y. Lam and B. Z. Tang, *Nanoscale*, 2021, **13**, 13610–13616.
11 L. He, D. Di, X. Chu, X. Liu, Z. Wang, J. Lu, S. Wang and Q. Zhao, *J. Controlled Release*, 2023, **363**, 180–200.
12 C. Y. Tsang and Y. Zhang, *Chem. Soc. Rev.*, 2024, **53**, 2898–2931.
13 X. Bai, Y. Yang, W. Zheng, Y. Huang, F. Xu and Z. Bao, *Mater. Chem. Front.*, 2023, **7**, 355–380.
14 X. Su, Y. Feng, H. Shi, F. Wang, Z. Wang, S. Hou, X. Song, J. Yang and L. Liu, *Int. J. Biol. Macromol.*, 2023, **239**, 124272.
15 S. Li, Q. Deng, Y. Zhang, X. Li, G. Wen, X. Cui, Y. Wan, Y. Huang, J. Chen, Z. Liu, L. Wang and C.-S. Lee, *Adv. Mater.*, 2020, **32**, 2001146.
16 M. S. Dar, T. A. Tabish, N. D. Thorat, G. Swati and N. K. Sahu, *APL Bioeng.*, 2023, **7**, 031502.
17 P. Zang, Y. Du, C. Yu, D. Yang, S. Gai, L. Feng, S. Liu, P. Yang and J. Lin, *Chem. Mater.*, 2023, **35**, 7770–7780.
18 X. Niu, Y. Zhu, C. Ding, J. Ma, P. Wei, Y. Lin, W. Fang, Q. He, C. Li, J. Cheng, J. Zou, L. Lin, X. Chen and D. Kang, *Adv. Funct. Mater.*, 2023, **33**, 2306778.
19 Y. Li, H. Qi, Y. Geng, L. Li and X. Cai, *Colloids Surf., B*, 2024, **234**, 113743.
20 S. Jia, Z. Li, J. Shao, H. Yuan, L. Li and L. Xu, *ACS Appl. Polym. Mater.*, 2022, **4**, 5275–5280.
21 H. Li, Q. Li, Y. Gu, M. Wang, P. Tan, H. Wang, L. Han, Y. Zhu, F. He and L. Tian, *Aggregate*, 2024, **5**(3), e528.
22 Z. Luo, R. Ma, Z. Chen, Y. Xiao, G. Zhang, T. Liu, R. Sun, Q. Zhan, Y. Zou, C. Zhong, Y. Chen, H. Sun, G. Chai, K. Chen, X. Guo, J. Min, X. Lu, C. Yang and H. Yan, *Adv. Energy Mater.*, 2020, **10**, 2002649.
23 E. Zhang, Y. Chen, F. Lv, Z. Zuo, F. He, Y. Li, Y. Huang, Y. Li and S. Wang, *CCS Chem.*, 2024, **6**, 641–651.

 